Eco-friendly Inorganic Molecular Novel Antiperovskites for Light-emitting Application

Jiawei Luo, [#] Qun Ji, [#] Yilei Wu, [#] Xinying Gao, Jinlan Wang and Ming-Gang Ju*

School of Physics, Southeast University, Nanjing 211189, China.

[#] These authors have contributed equally.

*E-mail: juming@seu.edu.cn

Supplemental Information

Computational Methods

For the selection of candidate elements, note that we cannot collect all the valence states of elements and their corresponding ionic radii from previous works. Therefore, the common ionic valence states of elements and their corresponding Shannon's ionic radii[1] are adopted the rigid sphere model to empirically estimate the formability of compounds in this study. For LFAPs, $X_3B[MN_4]$, $[MN_4]$ is a tetrahedral structure replacing a single anion in the traditional antiperovskites. We regard the tetrahedron as a large spherical shape and its circumferential spherical radius *r* as an equivalent replacement, leading to the newly proposed Goldschmidt tolerance factor *t* of the LFAPs from the restriction of the rigid sphere model (**Fig. 2**): $t = (r + r_X)/\sqrt{2}(r_B + r_X)$ and octahedral factor μ_1: $\mu_1 = r_B/r_X$. Where $t \leq 1$ and $\mu_1 \geq \sqrt{2} - 1$. For the tetrahedral structure, we define the tetrahedral factor μ_2 of the LFAPs: $\mu_2 = r_M/r_N$. By the principle of maximum contact and the principle of no small disturbance, when the four spheres N are tangent, and the sphere M is tangent to them in its cavity, it is the minimum value of r_M. The relation of radius *r* of outer cut sphere with positive four sides is: $r = r_N + r_M = \sqrt{6}/4\ a = \sqrt{6}/4 * 2r_N$, (**Fig. 2**) where *a* is the tetrahedral edge length, leading to $\mu_2 \geq 0.225$. Moreover, 20 LFAPs synthesized in the previous experiment works also are induced with three factors to tighten up range of the corresponding LFAPs (see **Table S2**). Therefore, considering experimental data, the range of corresponding tolerance factors are as follows: $0.811 \leq t \leq 0.899$, $1.040 \leq \mu_1 \leq 1.265$ and $0.263 \leq \mu_2 \leq 0.531$. In the case of mixed LFAPs, the average of ionic radii of B' and B'' ions, $r_B = 1/2(r_{B'} + r_{B''})$ is adopted.

Owing to lack of the research on antiperovskite with formula of $X_3B[MN_4]$, only small dataset with the reported antiperovskites of 20 are selected in this study. Noted that most of anions in the experimental works are halogens, resulting in unavoidable limitations to generation of novel antiperovskites with anions in other groups of the periodic table. Besides, empirical parameters in the rigid sphere models are mostly originated from Shannon's ionic radii basing on ionic bond. Since tetrahedrons connected by covalent bonds, such as $[CO_4]^{4-}$ sp^3 hybrid tetrahedron,[2] are not considered in this study.

Table S1. The combination of formal oxidation states of each element in $X_3B[MN_4]$. LFAPs are divided into four categories according to formal oxidation states of M ions.

Kind	M(valence)	N(valence)	X(valence)	B/ B´(valence)
1	+1	-1	+2	-3/-3
2	+2	-1	+1	-1/-1
3	+3	-2	+2	-1/-1
4	+4	-2	+2	-2/-2

Table S2. The t, μ_1 and μ_2 of previously reported antiperovskites. The ionic radii (r_M, r_N, r_B, r_X) are basing on the Shannon's ionic radii.[1]

Compound	Space group	r_M	$r_{N/B}$	r_X	t	μ_1	μ_2	Refs.
$Cs_3Br(HgBr_4)$	Pnma	0.96	1.96	1.74	0.891	1.126	0.490	3
$Cs_3Cl(HgCl_4)$	Pnma	0.96	1.81	1.74	0.898	1.040	0.530	4
$Cs_3I(HgI_4)$	Pbca	0.96	2.20	1.74	0.879	1.264	0.436	5
$Cs_3Br(CdBr_4)$	I4/mcm	0.78	1.96	1.74	0.856	1.126	0.398	6
$Cs_3I(CdI_4)$	Pnma	0.78	2.20	1.74	0.847	1.264	0.355	5
$Cs_3Cl(MnCl_4)$	I4/mcm	0.66	1.81	1.74	0.839	1.040	0.365	7
$Rb_3Br(MnBr_4)$	I4/mcm	0.66	1.96	1.61	0.838	1.217	0.337	8
$Cs_3Br(MnBr_4)$	I4/mcm	0.66	1.96	1.74	0.833	1.126	0.337	9
$Cs_3I(MnI_4)$	I4/mcm	0.66	2.20	1.74	0.826	1.264	0.300	5
$Tl_3Cl(FeCl_4)$	I4/mcm	0.63	1.81	1.59	0.838	1.138	0.348	9
$Cs_3Br(FeBr_4)$	I4/mcm	0.63	1.96	1.74	0.828	1.126	0.321	9
$Cs_3Cl(ZnCl_4)$	I4/mcm	0.60	1.81	1.74	0.827	1.040	0.331	10
$Rb_3Br(ZnBr_4)$	Pnma	0.60	1.96	1.61	0.826	1.217	0.306	11
$Cs_3Br(ZnBr_4)$	I4/mcm	0.60	1.96	1.74	0.822	1.126	0.306	12
$Cs_3I(ZnI_4)$	Pnma	0.60	2.20	1.74	0.815	1.264	0.273	13

$Cs_3Cl(NiCl_4)$	I4/mcm	0.55	1.81	1.74	0.817	1.040	0.304	14
$Tl_3Cl(CoCl_4)$	I4/mcm	0.58	1.81	1.59	0.828	1.138	0.320	9
$Cs_3Cl(CoCl_4)$	I4/mcm	0.58	1.81	1.74	0.823	1.040	0.320	9
$Cs_3Br(CoBr_4)$	I4/mcm	0.58	1.96	1.74	0.827	1.043	0.332	9
$Cs_3I(CoI_4)$	Pnma	0.58	2.20	1.74	0.811	1.264	0.263	15

Table S3. Comparison of computed bandgaps of $Ba_3I_{0.5}F_{0.5}(SbS_4)$, $Ba_3F_{0.5}I_{0.5}(InSe_4)$, $Ca_3O(SnO_4)$, and $Rb_3Cl_{0.5}I_{0.5}(ZnI_4)$ by using PBE, SCAN and HSE06 functional, respectively.

Compound	E_g^{PBE} **(eV)**	E_g^{SCAN} **(eV)**	E_g^{HSE06} **(eV)**
$Ba_3I_{0.5}F_{0.5}(SbS_4)$	1.41	1.56	1.96
$Ba_3F_{0.5}I_{0.5}(InSe_4)$	2.36	2.77	3.31
$Ca_3O(SnO_4)$	1.17	1.57	2.55
$Rb_3Cl_{0.5}I_{0.5}(ZnI_4)$	2.96	3.63	3.98

Table S4. The computed bandgaps of 49 eligible candidates by using SCAN functional.

Compound	E_g **(eV)**	**Compound**	E_g **(eV)**
$Sr_3O(SnO_4)$	1.5057	$Cs_3Br(MnBr_4)$	3.434
$Ca_3O(SnO_4)$	1.5692	$K_3F_{0.5}I_{0.5}(MnBr_4)$	3.455
$Ba_3F_{0.5}I_{0.5}(SbS_4)$	1.5696	$Rb_3Cl_{0.5}I_{0.5}(MnBr_4)$	3.479
$Ca_3N(LiF_4)$	1.5885	$K_3Br_{0.5}Cl_{0.5}(MnBr_4)$	3.508
$Ba_3O_{0.5}Se_{0.5}(SnSe_4)$	1.639	$K_3Cl(MnBr_4)$	3.521
$Ba_3O_{0.5}Se_{0.5}(SnS_4)$	2.1706	$Rb_3F_{0.5}I_{0.5}(MnBr_4)$	3.523
$Ba_3O_{0.5}S_{0.5}(SnS_4)$	2.2817	$Cs_3Cl_{0.5}I_{0.5}(MnBr_4)$	3.569
$Ba_3F_{0.5}I_{0.5}(InSe_4)$	2.7714	$Cs_3Cl(MnCl_4)$	3.588
$Ba_3F_{0.5}I_{0.5}(InS_4)$	3.2622	$Rb_3Br_{0.5}Cl_{0.5}(MnBr_4)$	3.626
$Ba_3O_{0.5}S_{0.5}(ZrS_4)$	2.03	$Rb_3Cl_{0.5}I_{0.5}(ZnI_4)$	3.6306
$Ba_3O_{0.5}S_{0.5}(HfS_4)$	2.064	$Rb_3Cl(MnBr_4)$	3.642

$Na_3F(MnF_4)$	2.636	$Rb_3Br(MnBr_4)$	3.66
$Cs_3Cl_{0.5}I_{0.5}(MnI_4)$	2.981	$Cs_3Br_{0.5}Cl_{0.5}(MnBr_4)$	3.697
$Rb_3Cl_{0.5}I_{0.5}(MnI_4)$	3.005	$Rb_3F_{0.5}I_{0.5}(ZnBr_4)$	3.7211
$Ca_3O(HfO_4)$	3.0501	$Cs_3Cl(MnBr_4)$	3.722
$Sr_3O(HfO_4)$	3.0698	$Cs_3I(ZnI_4)$	3.7486
$Cs_3Br_{0.5}I_{0.5}(MnI_4)$	3.07	$K_3Cl(MnCl_4)$	3.752
$Cs_3I(MnI_4)$	3.081	$Cs_3Cl_{0.5}I_{0.5}(ZnI_4)$	3.7553
$Ca_3O(ZrO_4)$	3.0826	$K_3Br_{0.5}Cl_{0.5}(MnCl_4)$	3.768
$Rb_3Br(MnI_4)$	3.089	$K_3Br_{0.5}Cl_{0.5}(ZnI_4)$	3.7716
$Cs_3Br_{0.5}Cl_{0.5}(MnI_4)$	3.136	$K_3Br_{0.5}F_{0.5}(MnCl_4)$	3.777
$Cs_3Br(MnI_4)$	3.136	$Cs_3Br_{0.5}I_{0.5}(ZnI_4)$	3.7831
$Sr_3O(ZrO_4)$	3.163	$Rb_3Br(ZnI_4)$	3.7933
$Ca_3O(TiO_4)$	3.3271	$K_3F_{0.5}I_{0.5}(MnCl_4)$	3.794
$Sr_3O(TiO_4)$	3.3816		

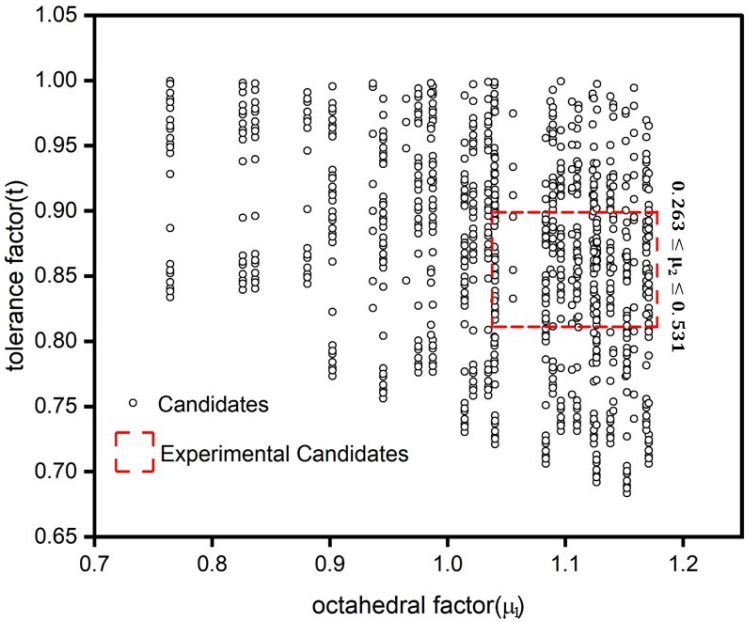

Figure S1. Candidate space with tolerance factor(t), octahedral factor(μ_1) and tetrahedron(μ_2) from the rigid sphere model. 266 candidates are further screened out with constraint range of experimental parameters.

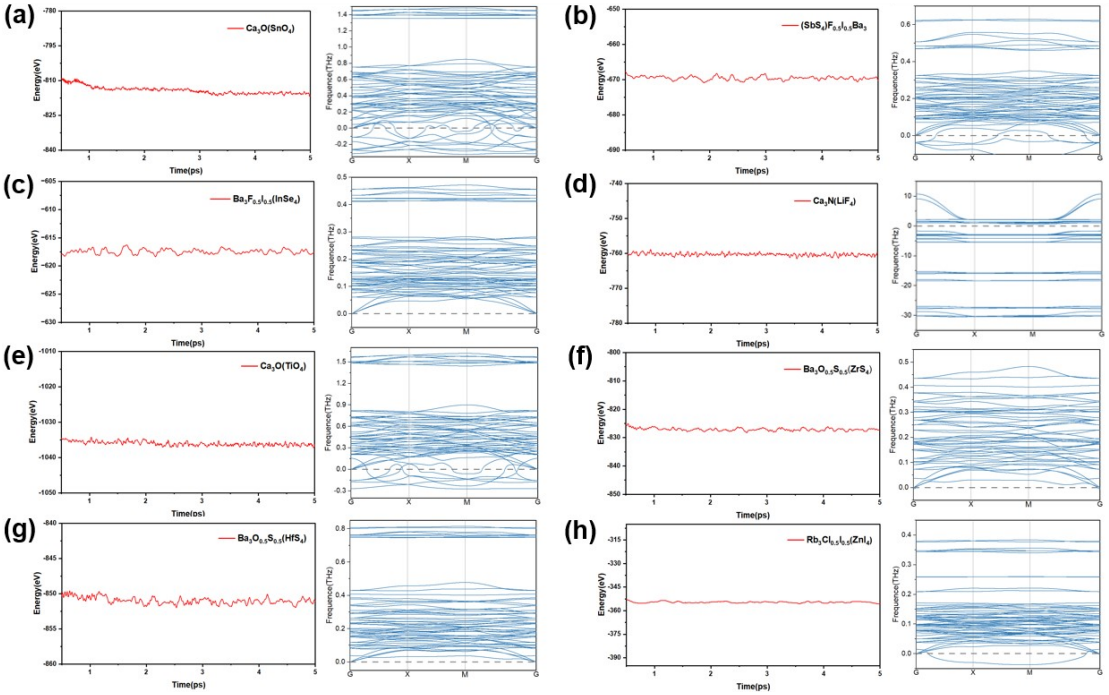

Figure S2. Simulations of AIMDs and phonon dispersion of (a) $Ca_3O(SnO_4)$, (b) $Ba_3I_{0.5}F_{0.5}(SbS_4)$, (c) $Ba_3F_{0.5}I_{0.5}(InSe_4)$, (d) $Ca_3N(LiF_4)$, (e) $Ca_3O(TiO_4)$, (f) $Ba_3O_{0.5}S_{0.5}(ZrS_4)$, (g) $Ba_3O_{0.5}S_{0.5}(HfS_4)$, and (h) $Rb_3Cl_{0.5}I_{0.5}(ZnI_4)$.

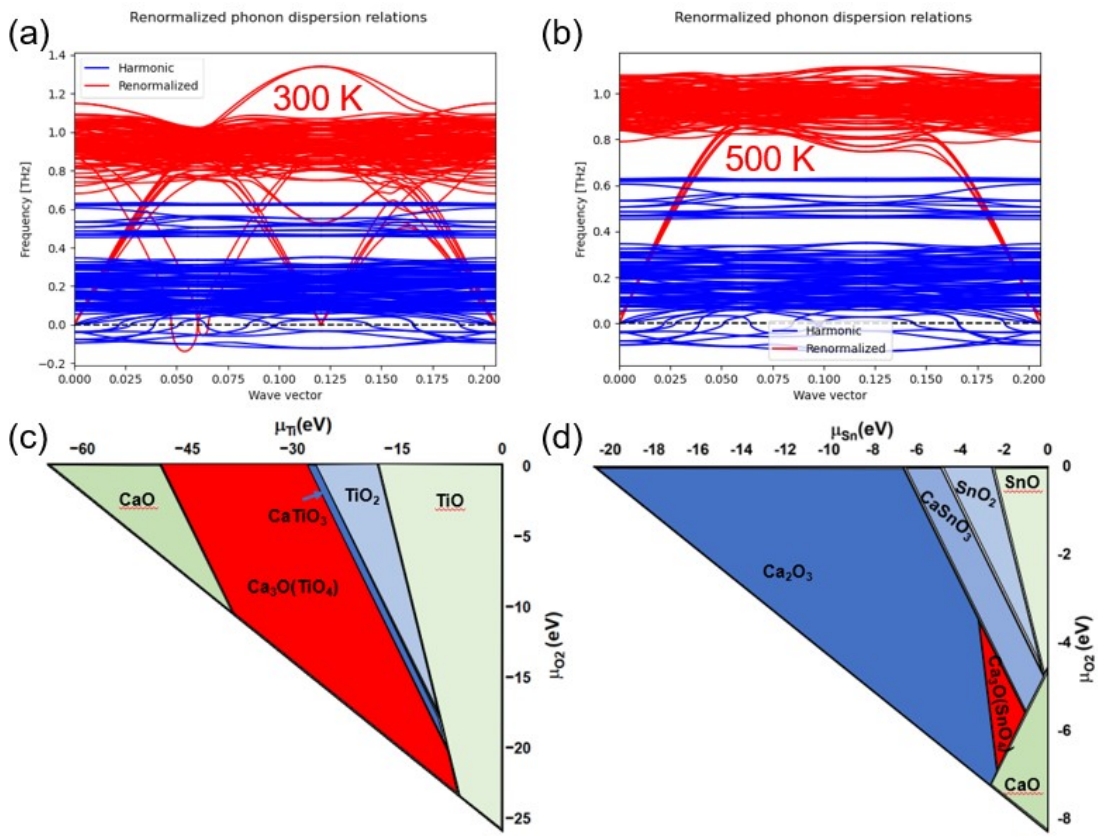

Figure S3. Harmonic phonon spectrum and renormalized phonon spectrum ((a) 300K and (b) 500K) with anharmonic terms for $Ba_3I_{0.5}F_{0.5}(SbS_4)$. The phase diagrams of (a) $Ca_3O(TiO_4)$ and (b) $Ca_3O(SnO_4)$, and the red region is the phase stable region.

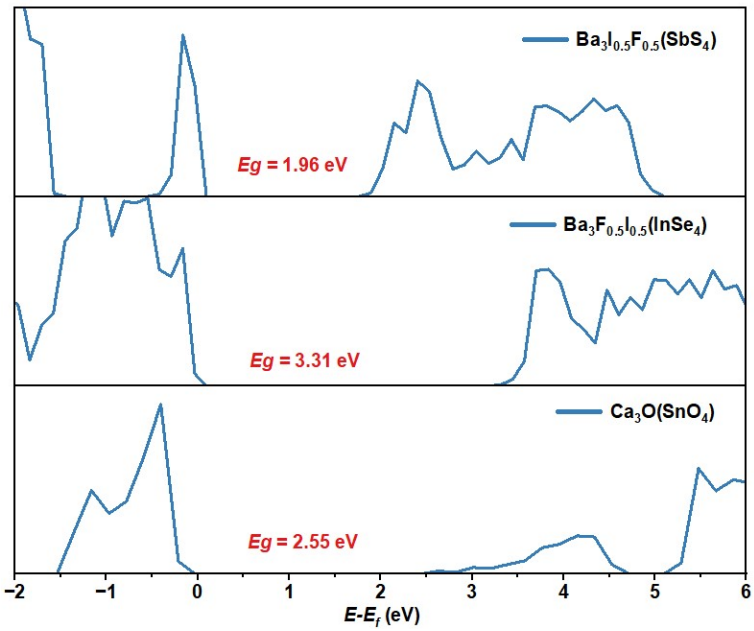

Figure S4. Computed DOSs of the $Ba_3I_{0.5}F_{0.5}(SbS_4)$, $Ba_3F_{0.5}I_{0.5}(InSe_4)$, and $Ca_3O(SnO_4)$ by using HSE06 functional.

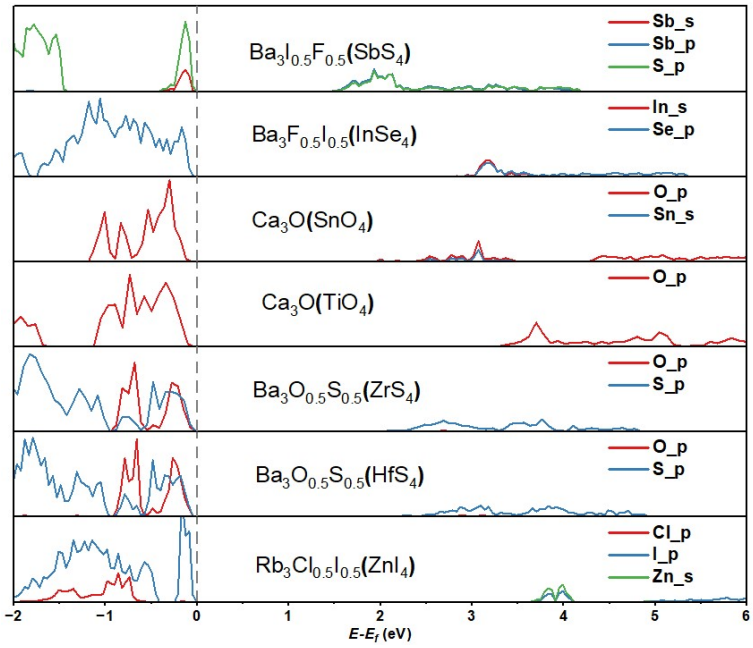

Figure S5. Computed PDOSs of $Ba_3I_{0.5}F_{0.5}(SbS_4)$, $Ba_3F_{0.5}I_{0.5}(InSe_4)$, $Ca_3O(SnO_4)$, $Ca_3O(TiO_4)$, $Ba_3O_{0.5}S_{0.5}(ZrS_4)$, $Ba_3O_{0.5}S_{0.5}(HfS_4)$, and $Rb_3Cl_{0.5}I_{0.5}(ZnI_4)$ by using SCAN functional.

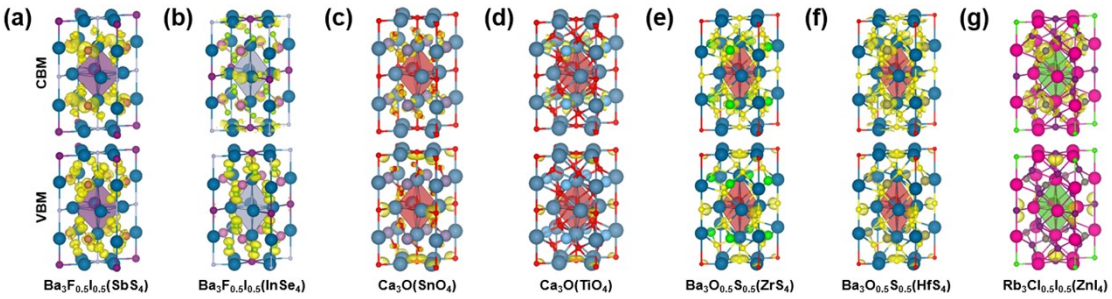

Figure S6. Spatial distributions of CBM and VBM of (a) $Ba_3I_{0.5}F_{0.5}(SbS_4)$, (b) $Ba_3F_{0.5}I_{0.5}(InSe_4)$, (c) $Ca_3O(SnO_4)$, (d) $Ca_3O(TiO_4)$, (e) $Ba_3O_{0.5}S_{0.5}(ZrS_4)$, (f) $Ba_3O_{0.5}S_{0.5}(HfS_4)$ and (g) $Rb_3Cl_{0.5}I_{0.5}(ZnI_4)$ by using SCAN functional.

Table S5. The hole and electron effective masses related to three orientations for candidates $Ba_3I_{0.5}F_{0.5}(SbS_4)$, $Ba_3F_{0.5}I_{0.5}(InSe_4)$, $Ca_3O(SnO_4)$, $Ca_3O(TiO_4)$, $Ba_3O_{0.5}S_{0.5}(ZrS_4)$, $Ba_3O_{0.5}S_{0.5}(HfS_4)$, and $Rb_3Cl_{0.5}I_{0.5}(ZnI_4)$ by using SCAN functional.

System	m_{e100}	m_{e010}	m_{e001}	m_{h100}	m_{h010}	m_{h001}
$Ba_3F_{0.5}I_{0.5}(SbS_4)$	1.164	1.044	0.494	1.515	4.320	2.055
$Ba_3F_{0.5}I_{0.5}(InSe_4)$	0.548	0.548	0.591	1.151	1.151	0.215
$Ca_3O(SnO_4)$	0.431	0.431	0.372	2.684	2.684	1.284
$Ca_3O(TiO_4)$	1.749	1.749	1.705	3.044	3.044	0.618
$Ba_3O_{0.5}S_{0.5}(ZrS_4)$	1.192	1.192	11.338	3.135	3.135	0.778
$Ba_3O_{0.5}S_{0.5}(HfS_4)$	1.032	1.032	3.186	2.883	2.883	0.764
$Rb_3Cl_{0.5}I_{0.5}(ZnI_4)$	0.532	0.532	0.371	11.629	11.629	2.870

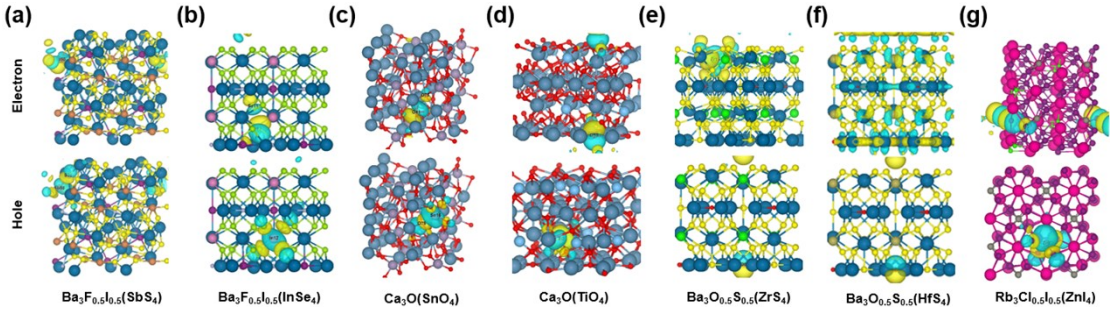

Figure S7. Spatial distributions hole and electron in the excited state of (a) $Ba_3I_{0.5}F_{0.5}(SbS_4)$, (b) $Ba_3F_{0.5}I_{0.5}(InSe_4)$, (c) $Ca_3O(SnO_4)$, (d) $Ca_3O(TiO_4)$, (e) $Ba_3O_{0.5}S_{0.5}(ZrS_4)$, (f) $Ba_3O_{0.5}S_{0.5}(HfS_4)$ and (g) $Rb_3Cl_{0.5}I_{0.5}(ZnI_4)$.

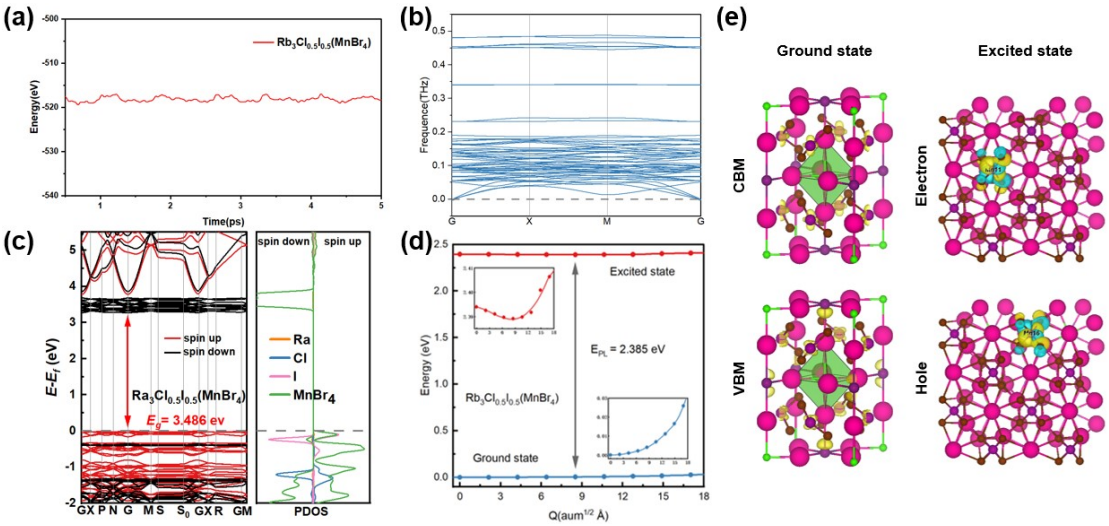

Figure S8. (a) Simulations of AIMD, (b) Phonon spectra, (c) band structure, (d) CCD, and (e) Spatial distributions for ground state and excited state of the candidate $Rb_3Cl_{0.5}I_{0.5}(MnBr_4)$.

REFERENCES

1 R. D. Shannon, *Acta Cryst A*, 1976, **32**, 751–767.

2 D. Spahr, J. König, L. Bayarjargal, P. N. Gavryushkin, V. Milman, H.-P. Liermann and B. Winkler, *Inorg. Chem.*, 2021, **60**, 14504–14508.

3 V. Pakhomov, P. Fedorov, G Sadikov, *Kristallografiya*, 1978, **23**, 615-616.

4 W. Clegg, Brown, M. L., L. J. A. Wilson, *Acta Crystallogr. B*, 1976, **32**, 2905-2906.

5 R. Sjövall, C. Svensson, *Zeitschrift Fur Kristallographie - Z KRISTALLOGR*, 1997, **212**, 732-741.

6 A. Kruglik, A. Vasil'ev, V. Grankina, G. *Kovalev, Crystallography*, 1992, **37**, 303-305.

7 J. Goodyear, D. Kennedy, *Acta Crystallographica Section B: Structural Crystallography and Crystal Chemistry*, 1976, **32**, 631-632.

8 H. J. Seifert, G. Flohr, *Zeitschrift für anorganische und allgemeine Chemie*, 1977, **436**, 244-252.

9 M. Amit, A. Horowitz, E. Ron, J. Makovsky, *Isr. J. Chem.*, 1973, **11**, 749-764. 35

10 K. Fejfarova, R. Ouarsal, B. El Bali, M. Dušek, M. Lachkar, *Acta Crystallographica Section E: Structure Reports Online*, 2007, **63**, i136-i137.

11 M. Heming, G. Lehmann, G. Henkel, B. Krebs, *Zeitschrift für Naturforschung A*, 1981, **36**, 286-293.

12 A. Kanishcheva, I. Y. Zaitseva, I. Kovalyova, Y. N. Mikhailov, *Russian Journal of Inorganic Chemistry*, 2010, **55**, 1882-1887.

13 K. Friese, G. Madariaga, T. Breczewski, *Acta Crystallographica Section C: Crystal Structure Communications*, 1998, **54**, 1737-1739.

14 M. Sassmannshausen, H. D. Lutz, *Acta Crystallographica Section C: Crystal Structure Communications*, 1998, **54**, 704-706.

15 D.-U. Des Phasendiagramms, D. Des Co, *Journal of Solid State Chemistry*, 1978, **26**, 397-

399.